energy was found to be 377.7 and 388.6 eV for the $j = 7/2$ and $5/2$ components, respectively—only 0.5 eV greater than that of uranium metal.

Photoemission spectra for the valence bands of these sublimed films showed strong uranium $5f$ emission, as expected given the high cross section of uranium $5f$ levels relative to carbon states in XPS. The formal valence state can be determined from uranium $5f$ emission centered at a binding energy of ~1.3 eV. The $5f$ signature was consistent with a formal 4+ valence state, in agreement with the assertion that a tetravalent atom has stabilized the fullerene.

The efficiency of formation of U@C_n metallofullerenes evident in these experiments is remarkable. Laser vaporization of freshly prepared graphite-UO_2 composite disks prepared simply by compression of the mixed pure powders were found to routinely produce cluster distributions similar to those of Fig. 4. The relative absence of empty fullerenes shown here suggests that fullerene cages are to some extent actually nucleated in the gas phase around uranium atoms or ions. In our experience, no other element has such a pronounced effect on the fullerene growth. We suspect that this is due to the strong complexing ability of uranium such as it is known to exhibit in uranocene (*18, 19*) and other similar compounds.

Further experiments showed that the use of a tetravalent internal metal atom to stabilize the C_{28} cage works to some extent with other elements as well. For example, zirconium was found to produce Zr@C_{28} in substantial yield as a result of the laser vaporization of a graphite-ZrO_2 composite target. Similar results have been obtained with hafnium and titanium. The relative abundance of the M@C_{28} cluster of these tetravalently stabilized metallofullerenes was in the order Ti@C_{28} << Zr@C_{28} < Hf@C_{28} < U@C_{28}. We suspect that this trend is due primarily to the better spatial overlap of the valence orbitals and the better energetic match of these orbitals for the larger central atom with the valence orbitals of the C_{28} cage. This notion is supported for the first two members of this series by SCF-RHF calculations on Ti@C_{28} and Zr@C_{28}, and we expect it will be borne out in future calculations of Hf@C_{28} and U@C_{28} with appropriate relativistic effective core potentials.

The C_{28} fullerene cage therefore appears to have the remarkable property of being tetravalent toward reactions both on the outside and on the inside. Considered as a tetrahedral unit, one can imagine C_{28} interlinked in many ways, including in a simple diamond lattice to form yet another new crystalline form of pure carbon. Our calculations show that the C_{28} unit can exhibit tetrahedral valence on the outside and on the inside simultaneously to form complexes such as (Ti@C_{28})H_4. A wide array of new molecules and materials may therefore ultimately be available if these C_{28} fullerene and M@C_{28} metallofullerenes are used as building blocks on a nanometer scale.

REFERENCES AND NOTES

1. R. F. Curl and R. E. Smalley, *Science* **242**, 1017 (1988); *Sci. Am.* **265**, 54 (October 1991).
2. V. Parasuk and J. Almlöf, *Chem. Phys. Lett.* **184**, 187 (1991).
3. L. A. Paquette, R. J. Ternansky, D. W. Balogh, G. J. Kentgen, *J. Am. Chem. Soc.* **105**, 5446 (1983).
4. Q. L. Zhang *et al.*, *J. Phys. Chem.* **90**, 525 (1986).
5. R. E. Haufler *et al.*, *Chem. Phys. Lett.* **179**, 449 (1991).
6. H. W. Kroto, *Nature* **329**, 529 (1987).
7. M. Feyereisen, M. Guotowski, J. Simon, *J. Chem. Phys.* **96**, 2926 (1992), and references therein.
8. R. Ahlrichs, M. Bär, M. Häser, H. Horn, C. Kolmel, *Chem. Phys. Lett.* **162**, 16 (1989).
9. G. E. Scuseria, *ibid.* **176**, 423 (1991).
10. T. Guo and G. E. Scuseria, *ibid.* **191**, 527 (1992).
11. See (*9*) for a detailed discussion of the basis sets and theoretical methods used in these calculations.
12. Efforts to synthesize this highly stable $C_{28}H_4$ hydrofullerene by addition of H_2 or some other hydrogen-bearing species at an appropriate stage in condensing carbon vapors are currently under way.
13. Y. Chai *et al.*, *J. Phys. Chem.* **95**, 7564 (1991).
14. J. H. Weaver *et al.*, *Chem. Phys. Lett.* **190**, 460 (1991).
15. R. D. Johnson *et al.*, *Nature* **355**, 239 (1992); H. Shinohara *et al.*, *ibid.* **357**, 52 (1992); C. S. Yannoni *et al.*, *Science* **256**, 1191 (1992); M. M. Alvarez *et al.*, *J. Phys. Chem.* **95**, 10561 (1991).
16. J. J. Pireaux *et al.*, *Chem. Phys.* **22**, 113 (1977).
17. J. Verbist, J. Riga,, J. J. Pireaux, R. Caudano, *J. Electron Spectrosc. Related Phenom.* **5**, 193 (1974).
18. A. H. H. Chang and R. M. Pitzer, *J. Am. Chem. Soc.* 111, 2500 (1989).
19. R. M. Pitzer and N. W. Winter, *J. Phys. Chem.* **92**, 3061 (1988).
20. We acknowledge helpful discussions with R. Pitzer and A. Rosen concerning the nature of uranium complexes and uranofullerenes. G.E.S. is a Camille and Henry Dreyfus Teacher-Scholar. This research was supported by the National Science Foundation, the Office of Naval Research, and the Robert A. Welch Foundation and made use of a laser-vaporization cluster beam FT-ICR apparatus supported by the U.S. Department of Energy. Office of Basic Energy Sciences, Division of Chemical Sciences.

5 May 1992; accepted 1 July 1992

Molecular Structure of the Coalescence of Liquid Interfaces

Joel Koplik and Jayanth R. Banavar

When two bodies of liquid merge, their interfaces must also rupture and rearrange into one. Virtually no information is available concerning the small-scale dynamics of this process. Molecular dynamics simulations of coalescence in systems of about 10,000 Lennard-Jones particles have been performed, arranged so as to mimic laboratory experiments on dense liquids. The coalescence event begins when molecules near the boundary of one liquid body thermally fluctuate into the range of attraction of the other, forming a string of mutually attracting molecules. These molecules gradually thicken into a tendril, which continues to thicken as the bodies smoothly combine in a zipper-like merger.

The coalescence of two drops of liquid is, on the whole, a problem of continuum fluid mechanics, but the fine structure of the rupture and the recombination of the drops' interfacial boundaries occur at the scale of molecules. Modeling based on the Navier-Stokes equation successfully captures the evolution of drop shape (*1–3*) but lacks a boundary condition or rule derivable from first principles for sewing two interfaces together. Typically, one might say that two interfaces have coalesced when they come within some prescribed (small) distance of each other, and one can then appropriately modify the boundary shape by hand if the subsequent time development is to be calculated. Such an approximation, however, does not allow one to identify cases where drops approach but coalescence does not occur and it also omits a number of potentially significant effects, such as fluctuations in stress as an interface ruptures or the formation of small satellite drops. Furthermore, a complete understanding of coalescence dynamics is invaluable for additional questions such as the entrainment of external fluid or vapor during splashes (*4*) or the disposition of contaminants or surfactants on the drop surface (*5*). More generally, one would like to know more about the microscopic dynamics of the process. We have addressed this question by calculations at the relevant length scale—that of individual molecules.

We consider molecules interacting by the familiar Lennard-Jones interaction (*6*),

$$V_{ij}(r) = 4\epsilon[c_{ij}(r/\sigma)^{-12} - d_{ij}(r/\sigma)^{-6}] \quad (1)$$

J. Koplik, Benjamin Levich Institute and Department of Physics, City College of New York, New York, NY 10031.
J. R. Banavar, Department of Physics and Materials Research Laboratory, Pennsylvania State University, University Park, PA 16802.

cutoff at 2.5σ, where i and j refer to the various liquids and solids in the system. In Eq. 1, r is the separation between a pair of molecules and σ and ϵ are length and energy scales, respectively. For a simulation involving a single species, one normally chooses $c = d = 1$, but here, as in earlier work on contact-line dynamics (7, 8), we maintain the coexistence of the various phases by choosing distinct values. We retain the standard coefficients for the intraliquid interactions, while immiscibility of two liquids is arranged by choosing $d_{12} = 0$, and the rigidity of the solid requires a deep and narrow potential with d_{ss} and c_{ss} chosen appropriately. In Fig. 1, we show the positions of the centers of the molecules for two drops suspended in a background fluid (not shown) between two solid plates. The simulation starts with the molecules in a face-centered cubic lattice; they are then equilibrated for a time interval 20τ ($\tau = \sigma\sqrt{m/\epsilon}$, where m is the common mass without flow at temperature $1.2\epsilon/k_B$ (k_B is the Boltzmann constant). The drops are out of the range of direct interactions with their periodic neighbors or the walls. There are 424 molecules per drop, 6352 in the background fluid and 1672 per plate, and the simulation box is 31σ by 26σ by 17σ, with periodic boundary conditions. Using typical "physical" values of the Lennard-Jones parameters, the linear size of the box is around 100 Å, and $\tau \approx 2 \times 10^{-12}$ s.

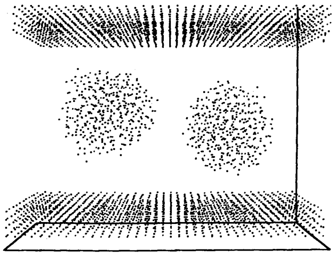

Fig. 1. Geometry for the coalescence of two liquid drops in shear flow. Two drops are surrounded by a second immiscible background fluid (not shown) between parallel plates after equilibration. The vertical line at the rear has length 26σ.

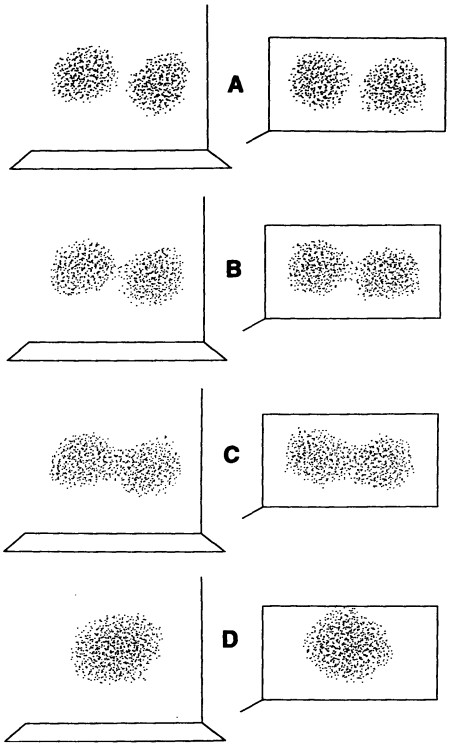

Fig. 2. Drop coalescence in shear flow, at times (**A**) 40, (**B**) 45, (**C**) 50, and (**D**) 110τ, shown in front and side views.

After equilibration, the two walls are translated parallel to themselves with opposite velocities $\pm 0.2\sigma/\tau$ so as to set up an approximately linear shear flow, which drives the drops together. The Reynolds number is ~0.5, and the Weber number is ~0.1. As the drops approach, thermal fluctuations cause molecules of one drop to move within interaction range of molecules of the other (Fig. 2). Such molecules are drawn together and in turn attract further drop molecules, producing a thin "filament" joining the two drops. The resulting dumbbell configuration has a rather high surface area and energy, which is reduced by the subsequent thickening of the filament and the eventual collapse of the drop molecules into a single sphere. In fact, once the connection is present, it is relatively easy to transport molecules between the two original drops, and the merger is relatively fast. We have also simulated drop merger in a molecular dynamics version of Taylor's four-roller mill (9), where typically a long time elapses until the initial contact of the drops whereupon the merger again requires a time on the order of 50τ.

In these calculations, the drops are relatively small (radius $\sim 5\sigma$), and shape distortions observed for nearby macroscopic drops are difficult to quantify. Furthermore, the velocity and stress fields are dominated by thermal fluctuations, and it is impossible to extract a boundary condition. Some improvement may be effected by considering the coalescence of a cylinder of liquid with a bath of fluid. In Fig. 3 we consider a cylinder of 2235 molecules, with radius 6σ and length 26σ falling under gravity ($g = 0.3\sigma/\tau^2$, with Reynolds and Weber numbers similar to those above) into a tank of 4500 molecules of the same liquid, again in the presence of an immiscible background fluid (not shown) and a solid plate at the bottom. Here, the falling cylinder must displace the background fluid, causing sub-

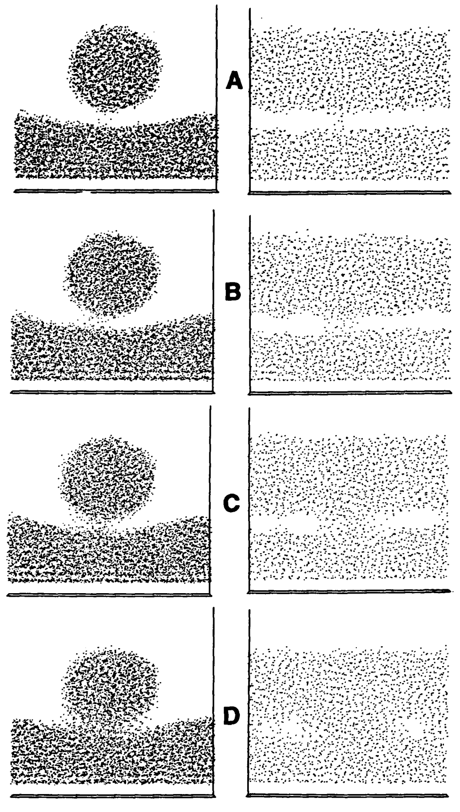

Fig. 3. Fall of a liquid cylinder into a bath under gravity, through an immiscible background fluid, which is not displayed. Times shown are (**A**) 40, (**B**) 42.5, (**C**) 45, and (**D**) 50τ. The side view represents a vertical section of width 5.65σ parallel to the axis of the cylinder.

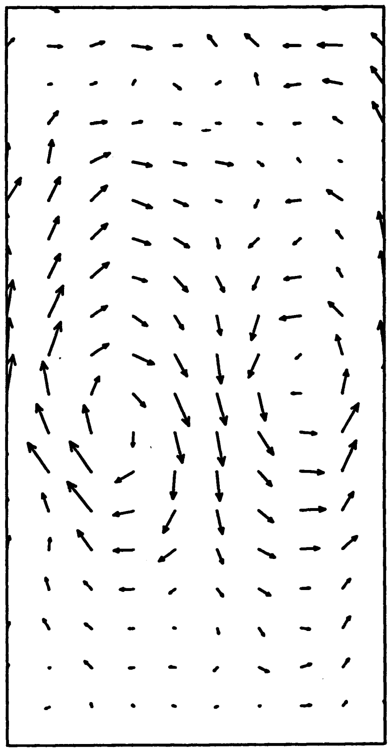

Fig. 4. Flow field corresponding to Fig. 3: velocity components in the plane perpendicular to the cylinder axis, averaged over the time interval $60\tau < t < 62.5\tau$ after the merger has occurred. The largest arrow shown corresponds to velocity $4.0\sigma/\tau$.

stantial distortion in the bath surface. As can be seen in the front and side views (Fig. 3), the initial contact again takes the form of a localized filament. As the cylinder approaches the bath, the filament thickens and the coalesced region moves outward from the point of first contact, zippering the two bodies of fluid together. This qualitative picture is also seen in a variety of other cylinder coalescence events we have simulated, including a weak four-roller flow, where the merger is driven for the most part by surface tension.

The Eulerian velocity field can be obtained by accumulating the average molecular velocities in a fixed array of sampling bins, averaged over the direction of the cylinder axis. The result (Fig. 4) shows the expected dipole vortex flow as the cylinder displaces bath fluid. At earlier and later times the velocity field indicates the drop descending and the bath fluid splashing upward, respectively. The dynamics of the splash, although interesting in itself (*10*), is awkward to study because a large bath is required and this is too costly in number of molecules and computer resources. The stress tensor has also been calculated in this flow but is too sensitive to thermal fluctuations to provide a clear signal.

The present set of simulations is, in a sense, on the edge of the continuum because average quantities such as shapes can be studied in detail, but the Navier-Stokes fields are often too noisy to resolve. Expected advances in computing power in the near future should overcome these difficulties, and we can look forward to systematic calculations of fluid phenomena on all interesting length scales.

REFERENCES AND NOTES

1. G. E. Charles and S. G. Mason, *J. Colloid Sci.* **14**, 105 (1960).
2. J. C. Lee and T. D. Hodgson, *Chem. Eng. Sci.* **23**, 1375 (1968).
3. G. V. Jeffreys and G. A. Davies, in *Recent Advances in Liquid-Liquid Extraction*, C. Hanson, Ed. (Pergamon, New York, 1971), pp. 495–584.
4. H. N. Oguz and A. Prosperetti, *J. Fluid Mech.* **203**, 149 (1989).
5. T. S. Sorensen, Ed., *Dynamics and Instability of Fluid Interfaces* (Springer-Verlag, New York, 1979).
6. M. P. Allen and D. J. Tildesley, *Computer Simulation of Liquids* (Oxford Univ. Press, Oxford, 1987).
7. J. Koplik, J. R. Banavar, J. F. Willemsen, *Phys. Fluids A* **1**, 781 (1989).
8. P. A. Thompson and M. O. Robbins, *Phys. Rev. Lett.* **63**, 766 (1989).
9. G. I. Taylor, *Proc. R. Soc. London Ser. A* **146**, 501 (1934).
10. A. M. Worthington, *A Study of Splashes* (Macmillan, New York, 1963).
11. This research was supported by the National Aeronautics and Space Administration Microgravity Program and the National Science Foundation Fluid, Particulate, and Hydraulic Systems Program, and the facilities of the Pittsburgh Supercomputer Center.

8 May 1992; accepted 7 July 1992

Rapid Intraplate Strain Accumulation in the New Madrid Seismic Zone

Lanbo Liu, Mark D. Zoback, Paul Segall*

Remeasurement of a triangulation network in the southern part of the New Madrid seismic zone with the Global Positioning System has revealed rapid crustal strain accumulation since the 1950s. This area experienced three large (moment magnitudes >8) earthquakes in 1811 to 1812. The orientation and sense of shear is consistent with right-lateral strike slip motion along a northeast-trending fault zone (as indicated by current seismicity). Detection of crustal strain accumulation may be a useful discriminant for identifying areas where potentially damaging intraplate earthquakes may occur despite the absence of large earthquakes during historic time.

The rate at which elastic strain energy accumulates controls how often large earthquakes can occur. Although strain rates in intraplate regions must, in general, be quite low (*1*), in areas such as the New Madrid, Missouri, and Charleston, South Carolina, seismic zones, strain rates must be relatively rapid if paleoseismic evidence indicating the occurrence of damaging earthquakes every 500 to 1000 years (*2, 3*) represents repeated slip on the same faults (*4*). In this study, we report measurements of the crustal strain accumulation rate in a portion of the New Madrid seismic zone (NMSZ). Historically, the NMSZ is the most active seismic zone in the midcontinent region east of the Rocky Mountains in the United States (*5*). Three large earthquakes occurred in December 1811 and January and February 1812. The estimated moment magnitudes (M) were all between M = 8.1 and M = 8.3 (*6*). We studied an area located along an approximately 100-km zone of seismicity (*7*) that trends to the northeast between Marked Tree, Arkansas, and Caruthersville, Missouri (Fig. 1). This zone coincides with a reactivated fault zone detected by seismic reflection profiling (*8*); the fault zone is centered along a major crustal rift originally formed in late Precambrian to early Paleozoic time (*9*). The inferred patterns of ground shaking and damage suggest that at least one (and possibly two) of the three major 1811 and 1812 earthquakes (indicated by the large gray dots in Fig. 1) were located along this segment of the NMSZ (*10*). Focal plane mechanisms of recent minor earthquakes indicate that overall motion is right-lateral strike slip along this fault trend (*11*). The result is consistent with the east-northeast to west-southwest direction of maximum horizontal stress in this region (*12*).

First- and second-order triangulation networks were established in this area as early as 1929 for engineering and mapping purposes. In the early 1950s, a much wider area was surveyed with the use of first- and second-order triangulation (*13*). Although crustal deformation can be measured with repeated angle measurements from the triangulation data alone (*14*) [as in (*4*)], there were insufficient repeated angles in this region to compute strain. We conducted a new survey of many of the triangulation stations with the Global Positioning System (GPS) in 1991. This made it possible to determine whether detectable crustal strain had accumulated during the past 35 to 40 years. With the use of dual-frequency GPS receivers, relative distances between bench marks can generally be determined to within several millimeters over the approximately 10-km baselines of the original triangulation network (*15*). In contrast, the precision of first-order triangulation is equivalent to several centimeters over approximately 10-km baselines.

We visited about 100 stations to recover the bench marks from the old surveys and found that many of the bench marks had been destroyed by either road construction or cultivation. An interconnected network of about 20 stations was found in good condition to the west of the town of Caruthersville (hereafter termed the Caruthersville network) that straddled both the northeast-trending zone of seismicity and the northwest boundary of the rift (Fig. 1). Although some scattered seismicity falls along the rift boundaries, the rift boundaries are not well defined by instrumentally recorded seismicity (Fig. 1). Most of the bench marks in the Caruthersville network had been surveyed in either January 1953 or May 1955. A new GPS survey of this area was made in March and April 1991. Each station was occupied twice (2 to 3 weeks apart) for an approximately 6-hour recording session. In the case of four bench marks (solid triangles in Fig. 1), satellite visibility was restricted by trees and buildings; consequently, remote stations were used or

---

Department of Geophysics, Stanford University, Stanford, CA 94305.

*Also at U.S. Geological Survey, Menlo Park, CA 94025.